Bacterial viability on chemically modified silicon nanowire arrays

A. Susarrey-Arce,[*a] I. Sorzabal-Bellido,[a] A. Oknianska,[a] F. McBride,[a] A. J. Beckett,[b] J. G. E. Gardeniers,[c] R. Raval,[*a] R. M. Tiggelaar,[*c, d] Y. A. Diaz Fernandez,[*a]

Abstract: The global threat of antimicrobial resistance drives an urgent need for the design of novel antimicrobial strategies. Functional surfaces are essential to prevent spreading of infection and reduce surface contamination. In this study we have fabricated and characterized multiscale-functional nanotopographies with three levels of functionalization: (1) nanostructure topography in the form of silicon nanowires, (2) covalent chemical modification with (3-aminopropyl)triethoxysilane, and (3) incorporation of chlorhexidine digluconate. Cell viability assays were carried out on two model microorganisms *E. coli* and *S. aureus* over these nanotopographic surfaces. Using SEM we have identified two growth modes producing distinctive multicellular structures, *i.e.* in plane growth for E. coli and out of plane growth for *S. aureus*. We have also shown that these chemically modified SiNWs arrays are effective in reducing the number of planktonic and surface-attached microorganisms.

1. Introduction

Bacteria are one of the most abundant forms of life on our planet,[1] and display a natural tendency to adhere onto surfaces as a self-defence and proliferation mechanism.[2] After initial colonisation of the surface, bacterial colonies experience a change of the metabolic activity that ultimately leads to the formation of complex multicellular structures, known as biofilms, featuring a high level of defence against antimicrobial agents.[3]

Preventing bacterial adhesion on surfaces is a powerful strategy to control biofilm formation,[4] reducing contamination of indwelling medical devices,[5] assuring food security,[6] and developing antifouling coatings.[7] The emergence of antimicrobial resistance (AMR) as a global threat has focused efforts in creating advanced materials and surfaces that can reduce and resist bacterial colonization.Promising antibacterial properties have been shown using chemical[8-10] or physical[11-16] functionalities at surfaces. However, it is becoming increasingly clear that single approach strategies may be inadequate in combating bacterial attachment on surfaces, and there is an important need to create multifunctional systems that combine two or more approaches. Here we develop a material based on highly-oriented silicon nanowires (SiNWs) with three levels of functionalization, combining both nanotopographies and chemical functionalities. These hierarchical structures have demonstrated ability to work as scaffolds for living systems like mammalian cells,[17-20] to aid bacterial-energy conversion[21] and to facilitate molecular recognition.[22] However, bacterial adhesion, biofilm formation and survival on SiNWs remain relatively under-explored.[23-26] In this study we investigate the interaction and the viability of bacteria on SiNWs surfaces enhanced with different chemical functionalities, using model microorganisms *E. coli* and *S. aureus*.

2. Materials and Methods

2.1 Fabrication of SiNWs

SiNWs were fabricated on silicon substrates (*p*-type boron doped, (100)-orientation, resistivity 5-10 Ωcm, 100 mm diameter, thickness 525 µm, single side polished; Okmetic, Finland). Prior to further processing, the substrates were cleaned by immersion in fuming 100% nitric acid (UN2031; OM Group) for 10 min. and in boiling 69% nitric acid (BASF, 51153574) for 15 min., which was followed by rinsing in demineralized water and spin drying. A regular pattern of 10 mm × 10 mm samples was defined with UV-lithography, such that each sample comprised a centred area of 8 mm × 8 mm in which SiNWs were formed. After development, the patterned resist was post-baked for at least 10 min. at 120 °C in ambient air. In the lithographically patterned areas SiNWs were formed with a two-step metal assisted chemical etching (MACE) process.[27-30] A 50% aqueous HF (BASF-51151083) was diluted 5 times in in demineralized water (DI-water) to which $AgNO_3$ (Sigma-Aldrich, 99%) was added to a concentration of 0.005 M. In order to deposit Ag nanoparticles (AgNPs) on the exposed silicon areas, the patterned substrates are immersed (in the dark) in this solution for 1 min. Subsequently the substrates are directly loaded in a solution of DI-water, 50%-HF and H_2O_2 (BASF, 55316830) (volumetric ratio DI:HF: H_2O_2 = 77.5:20:2.5), and etched for 20 min. (in dark conditions – etch rate ca. 0.6 µm/min). After this, the substrates are rinsed with demineralized water. The AgNPs were removed by immersing the substrates in 69% nitric acid (HNO_3; BASF, 51153574) at room temperature for 65 h, which was followed by rinsing with DI-water. To ensure complete removal of traces of photoresist the substrates were cleaned in a Piranha-solution (a 3:1 volumetric mixture of sulphuric acid (H_2SO_4; BASF, UN 1830) and H_2O_2; temperature 95 °C, cleaning time 15 min.), after which they were rinsed in DI-water and dried with a nitrogen (N_2) flow. Finally individual samples of 10 mm × 10 mm were cut using a dicing machine (Disco DAD-321), during which process glass plates covered the topside of the silicon substrates to avoid damage and contamination of the SiNWs. From SEM images (see **Figure 1**) the length, diameter and spacing between adjacent SiNWs were estimated for deeper layers with an error of 1-σ.

2.2 Functionalization of SiNWs

Chlorohexidine digluconate (CHD) and (3-aminopropyl) triethoxysilane (APTES) were purchased from Sigma Aldrich and used to introduce active chemical functionalities on the SiNWs surfaces. For the experiments described in sections 2.3 and 2.4, four kinds of SiNWs surfaces were prepared: (a) clean SiNWs, (b) SiNWs functionalised with CHD, (c) SiNWs functionalised with APTES, and (d) SiNWs functionalised with both APTES and CHD. The SiNWs surfaces with no additional functionalisation were used after cleaning in 69% nitric acid. APTES functionality was introduced by

immersing the SiNWs in 2% APTES in absolute ethanol for 2 h at 50 ^{o}C; followed by washing with ethanol and drying for 1 h at 50 ^{o}C. CHD functionalisation was performed on clean SiNWs or SiNWs-APTES as required, by immersing the surfaces in aqueous solutions of CHD and allowing equilibration for 24h at room temperature, followed by 15min rinsing in DI-water, and air-drying at room temperature. For the experiments described in **section 2.3** and **2.4**, CHD loading concentration of 0.2%, 0.02%, and 0.002% were used for the planktonic cells tests, whereas 0.02% and 0.002% were used to analyse the cells attached to the surface.

2.3 Determination of bacterial cell viability after culture of *E. coli* and *S. aureus* over SiNWs functionalised surfaces

S. aureus (DSM-346) and *E. coli* (ATCC-10798) cultures were grown overnight (200 rpm, at 37 ^{o}C) in NB medium (Oxoid, Ltd-Thermo Fisher). The bacterial cells concentration was adjusted to 10^5 colony forming units per millilitre (CFU/mL) in sterile NB. Prior to microbiological assays, the surfaces investigated were immersed in 69% HNO_3 (Sigma-Aldrich) for 12 h and rinsed in DI water. pH was monitored to ensure complete HNO_3 removal. Final pH values were found between 6.5 and 7.5. The surfaces were then placed in 24-well cell culture plates and sterilized under UV light for 5 min. Then, each substrate was immersed in 1 mL of bacterial cell suspension and incubated at 37 ^{o}C for 0, 4, 8 and 24h for the determination of viability of planktonic cells, and 8 and 24h for the viability experiments on surfaces. At the end of each incubation period, CFU/mL colony counting of planktonic viable cells was performed Thereafter, SiNWs surfaces were washed 3 times with sterile 0.85% NaCl.

Cell viability of *S. aureus* and *E. coli* attached to SiNWs and to functionalised surfaces was analysed with Live/Dead BacLight Bacterial Viability kit (Molecular Probes, L7012). Briefly, all surfaces were stained for 30 min in the dark with 1 mL of sterile 0.85% NaCl solution containing mixtures of SYTO 9 green-fluorescent nucleic acid stain for live cells, and the red-fluorescent nucleic acid stain propidium iodide for dead cells (see **Scheme 1**). After staining, surfaces were rinsed with sterile Milli-Q water and immediately analysed using a confocal upright 880 multiphotone microscope. Collected images were analysed with a home-made script employing Fiji software.

2.4 Scanning electron microscopy of bacterial cells attached to SiNWs functionalised surfaces

Scanning electron microscopy (SEM) samples were initially processed as described in **section 2.3**, and fixed overnight at 4°C with 4% paraformaldehyde and 2.5% glutaraldehyde in 0.1M phosphate buffer. Subsequent fixation and staining were carried out in water using 2% osmium tetroxide for 1 h, 1% tannic acid for 30 min., and 2% osmium tetroxide for 1h. Between each step, the samples were abundantly rinsed with DI-water. Finally, staining overnight at 4 °C with 1% uranyl acetate in water was performed. After staining, the samples were rinsed with DI-water, and progressively dehydrated with different volumetric ratios of ethanol (*i.e.* 30%, 50%, 70%, 90% and 100%). After dehydration, SiNWs samples were critical-point dried in CO_2 (Quorum Technologies K850) and sputter coated with 10 nm of AuPd (Quorum Technologies Q150T) for subsequent SEM imaging at 10 keV with JEOL SEM 7001.

3. Results and discussions

Functional antibacterial surfaces can be classified into two main areas: (1) nanotopographic surfaces with intrinsic antibacterial properties, and (2) surfaces displaying chemical functionalities with biocidal effect.[10, 11, 16] The combination of these two strategies may lead to a new generation of hierarchical multifunctional surfaces. To explore their potential, we have selected vertically aligned SiNWs as starting material with a defined topography and high surface area (see **scheme 1(I)**). We have added to these surfaces the chemical functionality APTES (see **scheme 1(II)**) which is frequently used in modification of biocompatible surfaces.[31] Furthermore, exploiting the high surface area of our fabricated nanoarchitectures, we have used the SiNWs-APTES materials as carrier for the loading/release (see **scheme 1(III)**) of the biocide chlorohexidine digluconate (CHD). Bacterial viability of cells in the planktonic state and attached to surfaces was investigated and the individual effect of each functionality is described below.

3.1 SiNWs nanotopographies

Our SiNWs fabrication protocol is able to create nanotopographic structures on flat silicon wafers using a two-step metal assisted chemical etching process.[27-30] An array of vertically aligned SiNWs connected at the base with the silicon wafer is obtained over a large area (*i.e.* 0.64 cm^2). From SEM characterization in **Figure 1**, the thickness of 11.3 ± 0.2 µm for the SiNWs-layer was estimated. The top of each nanowire is observed to be slightly tapered, sharpening over a length of *ca.* 0.7-1.1 µm. The diameter and spacing between adjacent SiNWs are 143 ± 24 nm and 77 ± 16 nm, respectively. Top view SEM-images (**Figure 1(b)**) reveal that the SiNWs are slightly bent towards neighbouring wires. In fact, the tops of adjacent SiNWs clump together, forming a cauliflower-like pattern across the entire surface of the sample, which we refer to as 'regular crowding of SiNWs' (**Figures 1(a)** and **(b)**). Side-view SEM images reveal that the SiNWs structures display a high surface area (**Figure 1**). Chemical composition of these surfaces was investigated using XPS) and the results show that the surface is mainly composed of SiO_2 (*ca.* 78%, see **ESI section 1**). We have also determined the water contact angle of 12^{o} for the as-synthesized surfaces. After overnight cleaning with nitric acid, the contact angle was 5^{o}, indicating that the surface is hydrophilic (**ESI section 1**).[32]

Comparable nanotopographies have been reported to have intrinsic antibacterial properties, attributed exclusively to morphological features.[11] To evaluate the potential antibacterial properties of SiNWs, we have investigated the bacterial viability of two model microorganisms *Escherichia coli* (*E. coli*, Gram negative, rod-like shape) and *Staphylococcus aureus* (*S. aureus*, Gram positive, round-like shape)[33, 34] on SiNWs arrays (**scheme 1**).

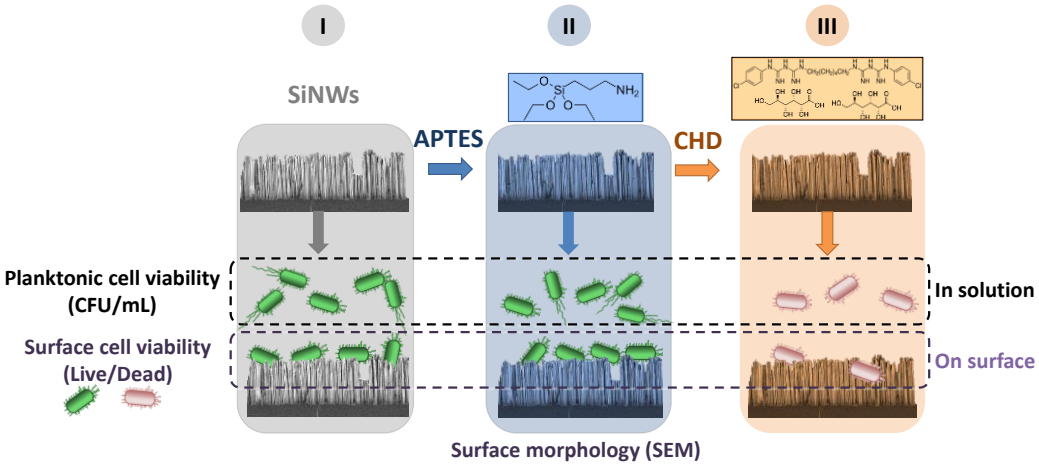

Scheme 1. Side-view SEM-images (false colour) of SiNWs (grey) functionalized with APTES (blue) and APTES loaded with CHD (orange). In the dashed open-black box: CFU/mL colony counting of planktonic viable cells cultured over SiNWs samples. Analysis of bacterial cell viability on surfaces (dashed open-purple box) was performed by Live/Dead staining followed by confocal microscopy. Morphology of attached cells attached to surfaces was examined by SEM.

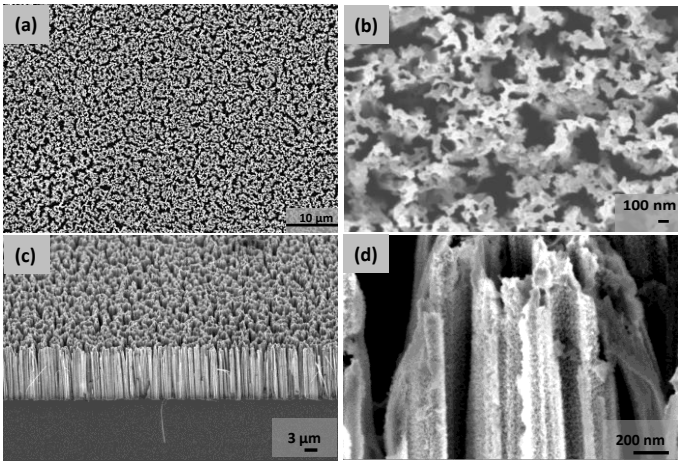

Figure 1. Representative SEM images of: (a-b) Top-view of SiNWs. (c-d) Side-view of SiNWs.

but measurable, antibacterial activity. Surface nanotopography has been proven to display intrinsic antibacterial properties as reported by Ivanova *et al* on black silicon surfaces,[11] where compromised bacterial cell membranes were observed,attributed to the formation of toroidal pores in a lipid bilayer.

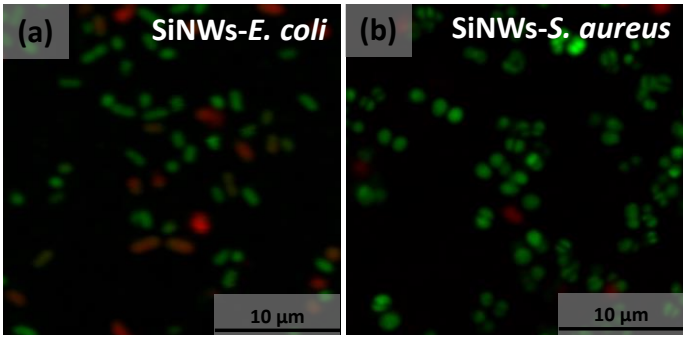

Figure 2. Representative merged confocal laser scanning microscope images for live (green), and dead (red) bacteria on SiNWs after 8h of culture: *E. coli* (a) & *S. aureus* (b).

3.1.1 Bacterial colonisation on SiNWs

Viability of cells attached to SiNWs arrays was investigated using Live/Dead staining as sketched in **scheme 1(I)**. Confocal microscopy images in **Figure 2** show that the majority of *E. coli* and *S. aureus* deposited cells remained alive (green) after 8h of culture over SiNWs, while a smaller amount of cells were identified as dead (red) as shown in **Figures 2**.

To generate additional insights on bacterial interaction with the surfaces, we have performed SEM analysis. **Figure 3** displays a side-view SEM image of *E. coli* on SiNWs, where intact, morphologically unchanged cells lay horizontally over the SiNWs surface. These results are in agreement with the viability data as shown in **Figure 2** demonstrating that nanofabricated surfaces display relatively low,

Our non-functionalised SiNWs arrays demonstrate lower antibacterial activity with respect to black silicon. This may be attributed to the differences in topography (*e.g.* structure height, diameter, and interspacing between structures) which represent a key factor in the surface performance.[15] SEM images of our SiNWs surfaces show relatively high wires density, with average wire-wire interspacing of 77nm. Under these conditions, both *E. coli* and *S. aureus* attach on top of the SiNWs arrays. This suggests that the effect of topography on bacterial attachment may be more complex than hitherto anticipated. Chemical composition could play also an important role on the antibacterial performance of these surfaces; Our SiNWs arrays contain up to 78% of SiO_2 (see **ESI data**). These differences suggest that both topography and surface chemistry

should be considered for the development of new nanostructured surfaces with antibacterial properties.

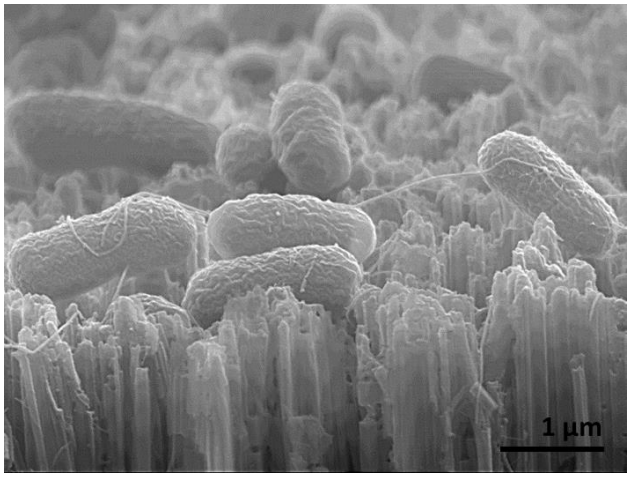

Figure 3. Representative side-view SEM image of *E. coli* on culture for 8 h over SiNWs.

3.2 Bacterial attachment on SiNWs–APTES surfaces

Functionalization of silicon oxide surfaces with silanes for biological applications is well known and has been previously discussed in the literature.[35] APTES is a small molecule that can be used to covalently bind biologically active molecules to SiO_2 surfaces. Here, we functionalized SiNWs surfaces with APTES to incorporate chemical functionalities to our nanotopographies as shown in **Scheme 1(II)**.

Live/Dead viability assays on cells attached to the surface of SiNWs-APTES (**Figure 4**) show similar results to experiments obtained with non-functionalized SiNWs. Bacteria are able to survive and colonise the surface, irrespective of APTES functionalisation. These results suggest that the SiNWs arrays modified with APTES also have a relatively low intrinsic antibacterial activity, and that the presence of APTES does not significantly alter the bacterial viability.of the SiNWs arrays..

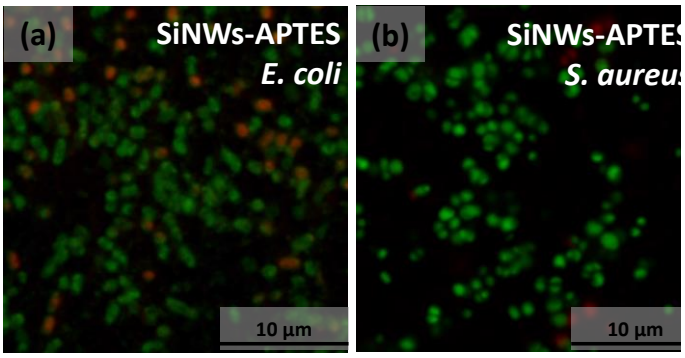

Figure 4. Representative merged confocal laser scanning microscope images of live (green) and dead (red) bacteria on SiNWs-APTES after 8h of culture: (a) *E. coli* & (b) *S. aureus*.

3.2.1 Growth modes of *E. coli* on SiNWs and SiNWs-APTES

SEM characterisation of bacteria attachment to SiNWs and SiNWs-APTES surfaces was also carried out. The sample preparation protocol preserves the morphology of the attached cells and extracellular matrix components involved in attachment with a high level of detail. High magnification SEM images on *E. coli* samples (**Figure 3**) show that the rod-like cells lie horizontally on the SiNWs arrays, without compromising cell morphology. The results from SiNWs-APTES, **Figure 5,** were also similar, suggesting that the APTES functionality does not alter cell behaviour. Direct interaction of cells with the surface appears to be favoured in both cases, producing in plane 'two-dimensional (2D)' bacterial colonies. From SEM images, we do not observe dramatic cell damage induced by interaction with the sharp features of SiNWs arrays (**Figure 3** and **5**)..

The morphology of the colonies may be associated with both the interaction of *E Coli* with the surface and the growth mode of *E. coli*. In Gram negative *E. coli* many adhesins are displayed on pili or fimbriae, which are hair-like appendages on bacterial cells that allow single bacterial cells to attach to surfaces. The SEM image in Figure 3 shows that *E. coli* cells take advantage of flagella and pili to attach to sharp tips and cavities to colonise the surface. These extracellular structures and the rod-like shape of *E. coli* cells can generate multiple contact points with the irregular SiNWs arrays, as observed in our SEM data and as reported on other surfaces[39].

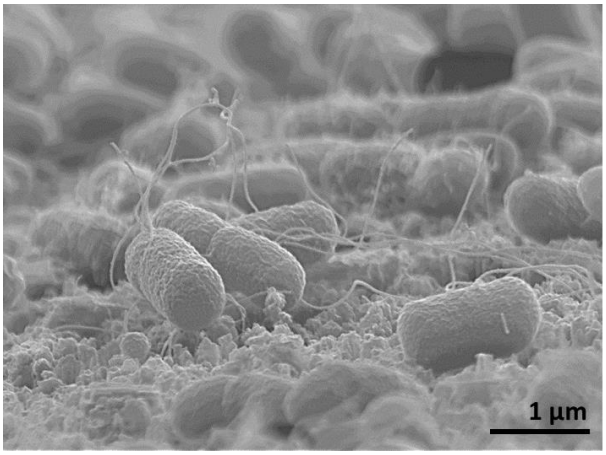

Figure 5. Representative side-view SEM image of E. coli on SiNWs functionalized with APTES after 8h of culture.

We hypothesize that after initial attachment, *E. coli* cells predominantly align and orientate parallel to the surface plane due to multiple bacteria-surface anchoring points as shown in **scheme 2**(**a**) and SEM images in **Figures 3 & 5**, and **ESI Figure S3**. Furthermore, *E Coli* cells display a symmetric rod-like shape[36, 37] with a single polar axis and are known to undergo lateral growth following the direction of the polar axis[37, 38] Therefore, preferential orientation of *E. coli* parallel to the surface plane would directly lead to '2D structures'. Interestingly, *E. coli* cells on flat silicon surfaces (**ESI Figure S3**) also display similar morphological structures, suggesting that these bacteria can accommodate to a

range of surfaces, with the rods preferentially aligning along the surface plane. Live-dead assays on the flat Si surfaces, however, show no kill, suggesting that the small bactericidal activity observed in the SiNW and APTES-functionalised SiNW arrays can be attributed to the nanotopography.

3.2.2 Growth modes of *S .aureus* on SNWs and SiNWs-APTES

In contrast to *E. coli* cells, *S. aureus* colonies on SiNWs and SiNWs-APTES surfaces develop vertically out of the plane, displaying only a few contact points with the surface as shown in **Figure 6**. Colonies show preferential out of the plane growth (see **Figure 6(d)**, scheme **2(b)**). *S. aureus* displays a cell membrane composed of a thick peptidoglycan layer that provides higher rigidity,[38-39] preventing the cells from adapting to surface topographies.

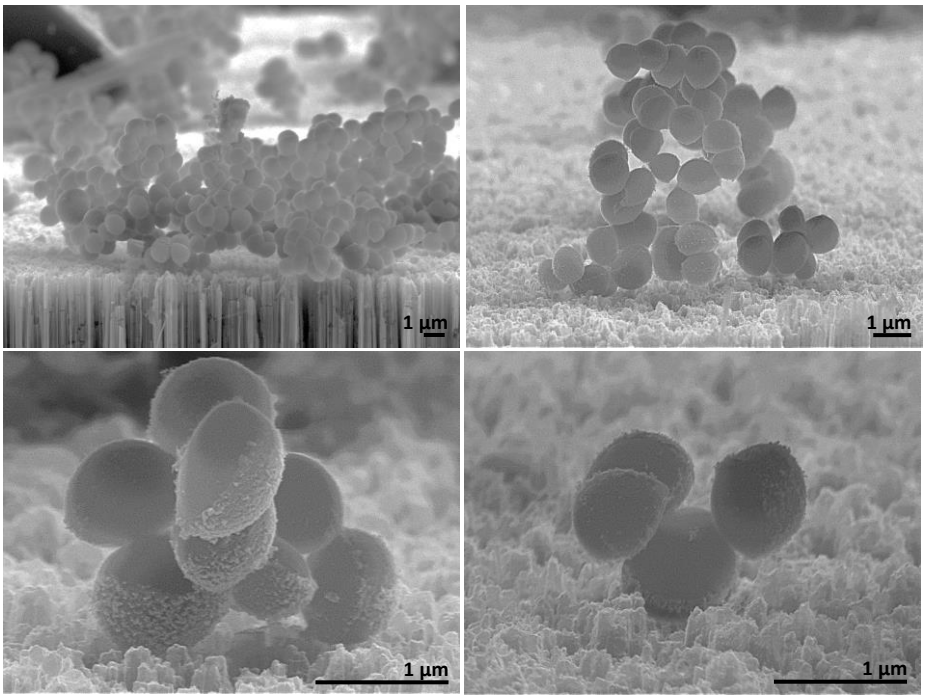

Figure 6. Representative side-view SEM image of *S. aureus* on SiNWs functionalized with APTES after 8h of culture. Interestingly, even very small colonies and delicate three-dimensional structures are able to resist sample processing for SEM, suggesting that cell/cell and cell/surface interactions are relatively strong.

S. aureus attachment on surfaces can be mediated by adhesins covalently anchored to the cell wall, allowing cell-cell, and cell-surface attachment. The round shape of the cell allows small contact areas to irregular surfaces like SiNWs arrays (**Figure 6**, **Figures S4**). Therefore, multi-cellular anchoring for neighbouring cells results morphologically difficult on SiNWs topographies for a round cell like *S. aureus*, allowing vertical growth of cells colonies on SiNWs arrays, as shown in **Scheme 2(b)**. Conversely, on flat silicon, *S. aureus* can display more contact points with the surface (**Figure S5**). These results suggests that surface topography may influence the out of the plane growth in *S. aureus*. Likewise, bacterial growth along the SiNWs surface could be partially hindered by the topographical features, leading to S. aureus colony growth out of the surface plane.

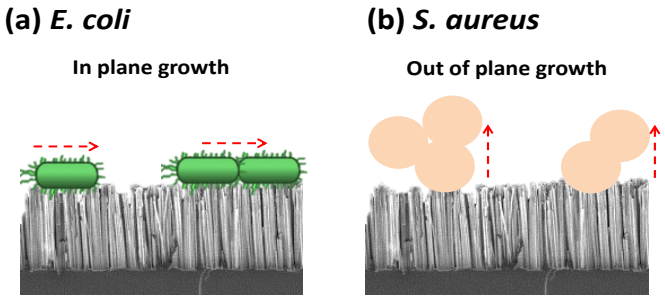

Scheme 2. Representation of bacterial growing modes on SiNWs & SiNWs-APTES surfaces: (a) *E. coli* and (b) *S. aureus*

3.3 SiNWs surfaces for biocidal release: cell viability on SiNWs and SiNWs-APTES arrays functionalised with CHD

The high surface area of SiNWs arrays shown in **Figure 1**, makes them good candidates for carrying bioactive cargos.[18-20] We have exploited this property to add a third level of functionalisation to SiNWs surfaces by using chlorhexidine digluconate (CHD), which is widely employed as a surface disinfectant and topical antibacterial agent.[40-41] Considering that CHD can be released from the surface, we initially hypothesised that it may affects the viability of cells

directly attached to the surface, as well as of planktonic cells dispersed in the liquid medium. In the next sections, we have studied the effect of CHD functionalisation, evaluating the antibacterial activity against *E. coli* and *S. aureus* in the planktonic state. Subsequently, the cell viability of surface attached *E. coli* and *S. aureus* was evaluated using live/dead staining, according to the strategy described in **Scheme 1(III)**.

3.3.1. Planktonic cell viability on SiNWs and SiNWs-APTES arrays loaded with CHD

We have considered two key factors influencing the antimicrobial properties of our surfaces: a) the loading capacity of the porous surface, and b) the released concentration of CHD over time into the liquid medium. Generally, the amount of material at the surface is negligible with respect to the liquid environment. Therefore, low loading capacity can lead to depletion of the cargo before reaching a critical microbicidal concentration, while excessively high loading causes unnecessary release of biocide to the environment, having a negative impact on the emergence of AMR. On the other hand, a relatively fast release of the cargo could deactivate the surface, allowing recolonization; while for relatively slow release, the biocide concentration over time might not be sufficient to exhibit antibacterial activity. Therefore, an optimal balance between cargo loading and release rate is necessary to deliver optimal performance of the antimicrobial surfaces.

In order to evaluate the effects of these factors on the released concentrations of CHD from SiNWs and SiNWs-APTES surfaces, we have performed a multi-level assay by varying the initial loading concentration of CHD from 0.002% to 0.2%, and collecting kinetic values of CHD release into the bulk medium after 4h, 8h, and 24h. The released concentrations were evaluated using UV-Vis spectroscopy, exploiting the intense absorption peak of CHD at 255nm (ESI **Figure S6**), using the same volume/surface ratio employed in the bioassays (see experimental section for details). The CHD quantification limit for this method has been estimated as ~0.4 mg/L. We have observed no difference in the release from 4h to 24h, suggesting that the CHD release is completed within 4h. The final concentration of CHD released from SiNWs-APTES is higher than from SiNWs surfaces, see **Table 1**. In addition to these results, we have also determined the minimum inhibitory concentrations (MIC) of CHD for the bacterial strains, obtaining values of 0.3 mg/L for *E. coli* and 0.6 mg/L for *S. aureus*. Considering the release data from **Table 1**, we can conclude that the concentration of CHD released into the liquid medium is above the *E. coli* MIC value for both SiNWs and SiNWs-APTES samples using loading concentrations of 0.2%, whereas for loading 0.02%, only SiNWs-APTES exceeded the MIC values for *E. coli*. Conversely, for *S. aureus* only SiNWs-APTES loaded with 0.2% of CHD exceeded the MIC value, while 0.02% loading produced a released concentration nominally close to the MIC

.

Table 1. Release of CHD from surfaces at different loading concentrations after 4h in H_2O

Surface	SiNWs	SiNWs-APTES
CHD Loading	**Release**	**Release**
0.2%	0.52 mg/L	2.0 mg/L
0.02%	<0.4 mg/L	0.6 mg/L
0.002%[§]	<0.4 mg/L[§]	<0.4 mg/L[§]
[§]below the detection limit of CHD		

To assess antimicrobial activity of the released CHD in the planktonic state, we have determined the number of colony forming units (CFU/mL) for bacterial solutions cultured for 4h, 8h, and 24h over SiNWs and SiNWs-APTES loaded with various concentrations of CHD (see **Figure 7**). Internal control samples for 0h incubation were included in each set of experimental data (red bars in **Figures 7a-d**). The results presented in **Figure 7** demonstrate that in the absence of CHD, no significant difference in planktonic bacterial viability was observed between SiNWs and SiNWs-APTES surfaces for both *E. coli* and *S. aureus*, suggesting that, under our experimental conditions, functionalisation of the SiNWs arrays with APTES has no effect on the planktonic cells.

When the SiNWs-APTES arrays are functionalised with CHD, the different sensitivity of *E. coli* and *S aureus* is manifested. For high loading concentrations of 0.2% of CHD, both *S. aureus* and *E. coli* are completely killed (see **Figure 7** WAC0), consistent with the determination of CHD release of 2.0 mg/L, which is considerable higher than the MIC value of both microorganisms.

Lower CHD loadings eradicate planktonic *E. coli* on SiNWs-APTES-CHD, but failed to completely kill *S. aureus* in the planktonic state (**Figure 7** SiNWC0). These results are consistent with MIC values and CHD released concentrations in **Table 1**. Interestingly, for low loading concentrations, *S. aureus* revealed an initial biocidal effect from 0h to 8h, followed by an increase in the cell population by four orders of magnitude from 8h to 24h (**Figure 7b** samples SiNW-AC1 & SiNW-AC1). These results can be explained considering the antibacterial mechanism of action of CHD. *Cheung et al.* reported that CHD biguanide kills Gram positive and negative microorganism by affecting cell membrane permeability. These authors have also demonstrated that the killing effect increased at longer biocide exposure time leading to progressive deterioration of cell membrane.[41] We hypothesise here similar effects for CHD glutamate to explain the progressive reduction of bacterial population from 0h to 8h (**Figure 7(b)**). The cell regrowth observed from 8h to 24h can be attributed to the presence of live bacteria either attached to the surface or surviving in liquid medium. This explanation is consistent with the concentrations of CHD released from the surfaces for 0.02% or lower loading in **Table 1**, leading to concentrations of CHD in the growing medium close to or below the MIC value for *S. aureus*.

The planktonic viability assay also demonstrates that the functionalisation of SiNWs with APTES increases the antibacterial activity of the surfaces against planktonic cells, as expected from

the higher concentration of CHD released from SiNWs-APTES surfaces (**Table 1**). These results are also consistent with SEM data showing lower density of bacterial cells attached to the surface of SiNWs-APTES (**Figures 8)** with respect to SiNWs (**Figure 9**) for the same CHD loading concentration.

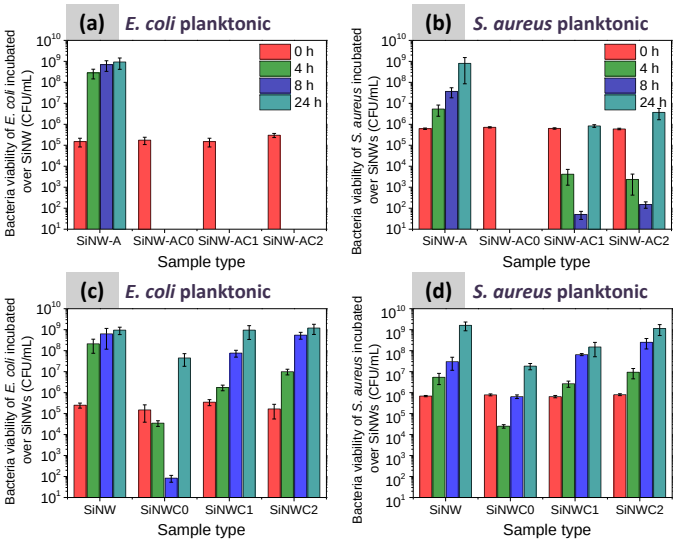

Functionalized surfaces in (a, b)	Code
SiNWs-APTES	SiNW-A
SiNWs-APTES with CHD 0.2%	SiNW-AC0
SiNWs-APTES with CHD 0.02%	SiNW-AC1
SiNWs-APTES with CHD 0.002%	SiNW-AC2

Non functionalized surfaces in (c, d)	Code
SiNWs	SiNW
SiNWs with CHD 0.2%	SiNWC0
SiNWs with CHD 0.02%	SiNWC1
SiNWs with CHD 0.002%	SiNWC2

Figure 7. Planktonic viability for *E. coli* and *S. aureus* after different culture times. Sample acronyms are listed within the table.

3.3.2 Bacterial viability on SiNWs & SiNWs-APTES arrays functionalised with CHD

From the planktonic viability data presented in **section 3.3.1**, we have identified SiNWs-APTES functionalised with CHD as our most promising candidate antibacterial surface. For this reason we have evaluated bacterial attachment on SiNWs-APTES and SiNWs-APTES functionalised with CHD using SEM imaging after different bacteria culture times. For each culture time SiNWs or SiNWs-APTES without CHD were used as a control. The results in **Figure 8** (**a, c, e**) show representative SEM images of *E. coli* and *S. aureus* cell attachment to the SiNWs-APTES arrays at 8 and 24h. The extent of surface attachment increases with the culture time, displaying low bacterial coverage up to 4 h (data not shown), while for longer culture times, dense bacterial colonies were observed along the surface.

On SiNWs-APTES arrays loaded with 0.02 % of CHD, SEM analysis demonstrates that for both *E. coli* and *S. aureus*, the number of cells attached to the surface after 8h is negligible compared to the SiNWs-APTES control (**Figures 8 a,b**). In the case of *E. coli*, the surface-based antibacterial activity was maintained up to 24h (**ESI-Figure S8**), while for *S. aureus*, we observe recolonization of the SiNWs-APTES arrays loaded with 0.02% CHD (**Figure 8f**). The surface recolonization after 24h is higher for S. aureus when lower loading concentrations of CHD are used, as shown in **ESI Figure S7**.

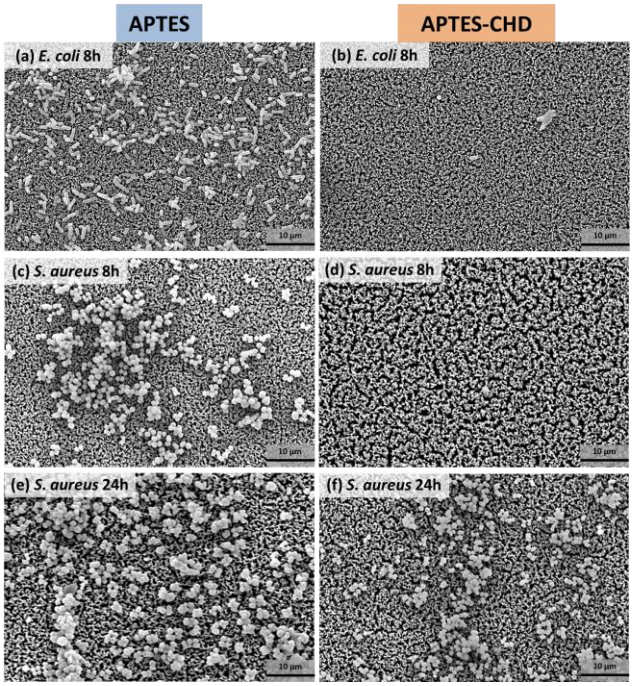

Figure 8. Representative top-view SEM image of *E. coli* after 8h of culture on (a) SiNWs-APTES, (b) SiNWs-APTES loaded with 0.02% CHD; *S. aureus* (c-f) on SiNWs-APTES after (c) 8h and (e) 24 h of incubation. *S. aureus* on SiNWs-APTES loaded with 0.02% of CHD after (d) 8h and (f) 24 h of culture.

Considering the dramatic difference observed between SiNWs and SiNWs-APTES during the planktonic experiments discussed in **section 3.3.1**, we have inferred that there may be also an effect of APTES functionalisation on the antibacterial activity against cells attached to these surfaces. To clarify this, we have investigated bacterial surface attachment on SiNWs-CHD (**Figure 9c-d**), and observed a considerable reduction of the number of cells attached to the SiNWs arrays in the presence of CHD. Nevertheless, the performance of these surfaces is apparently poor, if compare with the SiNWs-APTES-CHD counterparts at 8h (**Figure 8)**.

Following the strategy described in **Scheme 1 (III)**, we have quantified the biocidal effect on cells attached to SiNWs and SiNWs-APTES in the presence of CHD, to generate further insights on their antimicrobial activity. Viability of cells attached to the surface was determined by live/dead staining (**Figures 10 (a,b)**, ESI **Figures S9 & S10).** These results demonstrate that on SiNWs-APTES, despite *S. aureus* recolonization observed by SEM (**Figure 8)**, the fraction of live cells remains below 20% **(Figure 10b**, SiNW-AC1 & SiNW-AC2), suggesting that the viability of attached cells is strongly compromised. Interestingly, for loading concentrations of 0.02% (SiNW-AC1) the percent of live *S. aureus* cells on the surface remains below 5%.

For *E. coli* in **Figure 10**, the percent of viable cells on SiNWs-APTES surfaces loaded with CHD is systematically lower than for *S. aureus*, as expected from the higher sensitivity of *E. coli* to CHD. Similarly, for both bacteria, APTES functionalisation increases the antibacterial activity against attached cells. It is also interesting to

note that the intrinsic topological antibacterial effects of non-functionalised SiNWs and SiNWs-APTES account for 30%-60% reduction of bacterial viability, versus 10%-20% of dead cells on flat silicon (Si) and functionalised APTES silicon flat surfaces (Si-A).

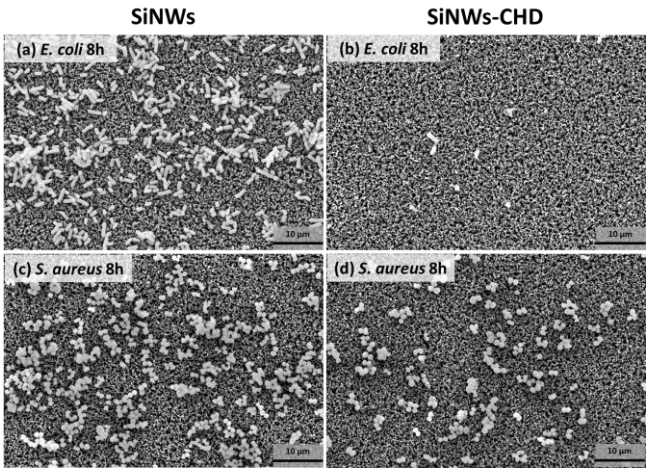

Figure 9. Representative top-view SEM image of *E. coli* and *S. aureus* after 8h of culture on (a-c) SiNWs and (b-d) SiNWs loaded with 0.02% CHD.

Comparing viability assays of cells in the planktonic state (**Figure 7**) and on the surface (**Figure 10**) we can confirm that in both cases *S. aureus* is less sensitive to CHD, as expected from the higher MIC values obtained in planktonic conditions (**Table 1**). Samples of SiNWs without APTES loaded with CHD (*i.e.* SiNWC1 & SiNWC2) were systematically less efficient against both *S. aureus* and *E. coli* than their SiNWs-APTES (SiNW-A) counterparts. The best antibacterial activity was observed for SiNWs-APTES functionalised with CHD (SiNW-AC1 & SiNW-AC2). On these SiNWs-APTES surfaces, the biocidal effect of CHD against attached cells was maintained after 24h, even when the antimicrobial activity against planktonic cells had declined. Interestingly, the viability of re-colonising *S. aureus* cells is strongly compromised, suggesting that a residual activity of CHD at the surface is still present.

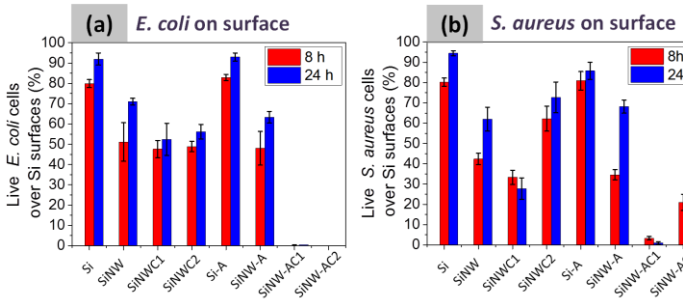

Figure 10. (a) *E. coli* and (b) *S. aureus* cell ratios determined with live/dead fluorescent staining. Samples acronyms are listed in **Figure 7**.

4. Conclusions

We have created a three level functionalised surface to study bacterial viability at each level of functionalisation on the surface and in planktonic state. Topographical structures in the form of SiNWs and SiNWs-APTES have some intrinsic antibacterial effect, but *E. coli* and *S. aureus* can still proliferate on these topographic surfaces. We have identified two different growth modes producing distinct in plane, and out of the plane bacterial colonies. Furthermore, we have incorporated an additional level of functionalisation with CHD displaying loading-dependent antibacterial properties. We have demonstrated the role of surface chemistry on the efficacy of these multifunctional surfaces. The presence of APTES modified the release of CHD, improving antibacterial activity of the SiNWs surfaces.

Acknowledgements

We would like to thank Dr. Marco Marcello, Dr. Joanna Wnetrzak and Dr. Dave Mason from the Liverpool Centre for Cell Imaging (CCI) for help with experimental design and image analysis support. We also acknowledge the support of University of Liverpool Biomedical Electron Microscopy Unit and Nanoinvestigation Centre at University of Liverpool (NICAL). Gareth Morris from the Open Innovation Hub for Antimicrobial Surfaces and Mattia Morassutto from Mesoscale Chemical Systems (MCS) are acknowledged for assistance in SiNWs-sample preparation. We also thank S. Schlautman (MCS) for sample fabrication and Gerard Kip (NanoLab) for XPS-analysis. This work was partly founded by EPSRC grant number EP/J019364/1.

References

1 N.C. Kyrpides, P. Hugenholtz, J.A. Eisen, T. Woyke, M. Göker, C.T. Parker, et al., Genomic encyclopedia of bacteria and archaea: sequencing a myriad of type strains, *PLoS Biol*, 2014, 12(8): e1001920
2 M. Wilkins, L. Hall-Stoodley, R. N. Allan, and S. N. Faust, New approaches to the treatment of biofilm-related infections, *Journal of Infection*, 2014, 69(S1), S47
3 H. Van Acker, P. Van Dijck, and T. Coenye, Molecular mechanisms of antimicrobial tolerance and resistance in bacterial and fungal biofilms, *Trends in Microbiology*, 2014, 22(6), 326
4 M. Simões, L. C. Simões, M. J. Vieira, A review of current and emergent biofilm control strategies, *LWT - Food Science and Technology*, 2010, 43(4), 573
5 Biofilms, medical devices, and antibiofilm technology: Key messages from a recent public workshop, *American Journal of Infection Control,* 2015, 43, 2
6 S. Srey, I. Kabir Jahid, and Sang-Do Ha, Biofilm formation in food industries: A food safety concern, *Food Control*, 2013, 31, 572e585
7 D. Shchukin, and H. Möhwald, A coat of many functions, *Science*, 2013, 341.6153, 1458
8 A. Agarwal, T. B. Nelson, P. R. Kierski, M. J. Schurr, C. J. Murphy, C. J. Czuprynski, J. F. McAnulty, and N. L. Abbott, Polymeric multilayer that localize the release of chlorhexidine from biologic wound dressing, *Biomaterials*, 2012, 33, 6783
9 Z. Zheng, X. Huang, M. Schenderlein, D. Borisova, R. Cao, H. Möhwald, and D. Shchukin, Self-healing and antifouling multifunctional coatings based on pH and sulfide ion sensitive nanocontainers, *Adv. Funct. Mater.*, 2013, 23, 3307
10 H. Gu, D. Ren, Materials and surface engineering to control bacterial adhesion and biofilm formation: A review of recent advances, *Front. Chem. Sci. Eng.*, 2014, 8(1), 20

11 E. P. Ivanova, J. Hasan, H. K. Webb, G. Gervinskas, S. Juodkazis, V. K. Truong, A. H.F. Wu, R. N. Lamb, V. A. Baulin, G. S. Watson, J. A. Watson, D. E. Mainwaring, and R. J. Crawford, Bactericidal activity of black silicon, *Nat. Comm.*, 2013, 4:2838

12 J. E. Gittens, T. J. Smith, R. Suleiman, R. Akid, Current and emerging environmentally-friendly systems for fouling control in the marine environment, *Biotechnology Advances*, 2013, 31(8), 1738

13 A. I. Hochbaum, and J. Aizenberg, Bacteria pattern spontaneously on periodic nanostructure arrays, *Nano Lett.*, 2010, 10(9), 3717

14 R. Vasudevan, A. J. Kennedy, M. Merritt, F. H. Crocker, R. H. Baney, Microscale patterned surfaces reduce bacterial fouling-microscopic and theoretical analysis, *Colloids and Surfaces B: Biointerfaces*, 2014, 117, 225

15 R. J. Crawford, H. K. Webb, V. K. Truong, J. Hasan, E. P. Ivanova, Surface topographical factors influencing bacterial attachment, *Advances in Colloid and Interface Science*, 2012, 179–182, 142

16 D. B. Weibel, W. R. DiLuzio, and G. M. Whitesides, Microfabrication meets microbiology, *Nature Reviews Microbiology*, 2007, 5, 209

17 W. Kim , J. K. Ng , M. E. Kunitake , B. R. Conklin , and P. Yang, Interfacing silicon nanowires with mammalian cells, *J. Am. Chem. Soc*., 2007, 129 (23), 7228

18 Alex K. Shalek, Jacob T. Robinson, Ethan S. Karp, Jin Seok Lee, Dae-Ro Ahn, Myung-Han Yoon, Amy Sutton, Marsela Jorgolli, Rona S. Gertner, Taranjit S. Gujral, Gavin MacBeath, Eun Gyeong Yang, and Hongkun Park, Vertical silicon nanowires as a universal platform for delivering biomolecules into living cells, *PNAS*, 2010, 107(5), 1870

19 Minsuk Kwak, Lin Han, Jonathan J. Chen, and Rong Fan, Interfacing Inorganic nanowire arrays and living cells for cellular function analysis, *Small*, 2015, 11(42), 5600

20 C. Chiappini, E. De Rosa, J. O. Martinez, X. Liu, J. Steele, M. M. Stevens and E. Tasciotti, Biodegradable silicon nanoneedles delivering nucleic acids intracellularly induce localized in vivo neovascularization, *Nature Materials*, 2015, 14, 532

21 C. Liu, J. J. Gallagher, K. K. Sakimoto, E. M. Nichols, C. J. Chang, M. C. Y. Chang, and P. Yang, Nanowire–bacteria hybrids for unassisted solar carbon dioxide fixation to value-added chemicals, *Nano Lett*., 2015, 15, 3634

22 N. N. Mishra, W. C. Maki, E. Cameron, R. Nelson, P. Winterrowd, S. K. Rastogi, B. Filanoski, and G. K. Maki, Ultra-sensitive detection of bacterial toxin with silicon nanowire transistor, *Lab Chip*, 2008, 8, 868

23 Q. Yu , H. Liu, and H. Chen, Vertical SiNWAs for biomedical and biotechnology applications, *J. Mater. Chem. B*, 2014, 2, 7849

24 K. K. Sakimoto, C. Liu, J. Lim, P. Yang, Salt-induced self-assembly of bacteria on nanowire arrays, *Nano Lett.*, 2014, 14 (9), 5471

25 L. Wang , H. Wang , L. Yuan, W. Yang , Z. Wu and H. Chen, Step-wise control of protein adsorption and bacterial attachment on a nanowire array surface: tuning surface wettability by salt concentration, *J. Mater. Chem*., 2011, 21, 13920

26 Elisabeth Galopin, Gaelle Piret, Sabine Szunerits, Yannick Lequette, Christine Faille and Rabah Boukherroub, Selective adhesion of bacillus cereus spores on heterogeneously wetted silicon nanowires, *Langmuir*, 2010, 26 (5), 3479

27 K. Q. Peng, H. Fang, J. J. Hu, Y. Wu, J. Zhu, Y. J. Yan, and S. Lee, Metal-particle-induced, highly localized site-specific etching of Si and formation of single-crystalline Si nanowires in aqueous fluoride solution, *Chem.-Eur. J.*, 2006, 12, 7942

28 S. Schmidt, S. Senz, and U. Gosele, Diameter-dependent growth direction of epitaxial silicon nanowires, *Nano Lett.*, 2005, 5, 931

29 C. Chartier, S. Bastide, and C. Levy-Clement, Metal-assisted chemical etching of silicon in HF-H_2O_2, *Electrochimica Acta*, 2008, 53, 5509

30 K. Peng, A. Lu, R. Zhang, and S. T. Lee, Mobility of metal nanoparticles in silicon and induced anisotropic silicon etching, *Adv. Funct. Mater.*, 2008, 18, 3026

31 M. S. A. Rahman, S. C. Mukhopadhyay, P.-L. Yu, J. Goicoechea, I. R. Matias, C. P. Gooneratne, J. Kosel, Detection of bacterial endotoxin in food: New planar interdigital sensors based approach, *Journal of Food Engineering*, 2013, 114, 346

32 H. Ems, S. Ndao, Microstructure-alone induced transition from hydrophilic to hydrophobic wetting state on silicon, *Applied Surface Science*, 2015, 339, 137

33 A. Taglietti, Y. A. Diaz Fernandez, E. Amato, L. Cucca, G. Dacarro, P. Grisoli, V. Necchi, P. Pallavicini, L. Pasotti, and M. Patrini, Antibacterial activity of glutathione-Coated silver nanoparticles against Gram positive and Gram negative bacteria, *Langmuir*, 2012, 28 (21), 8140

34 E. Amato, Y. A. Diaz-Fernandez, A. Taglietti†, P. Pallavicini, L. Pasotti, L. Cucca, C. Milanese, P. Grisoli, C. Dacarro, J. M. Fernandez-Hechavarria, and V. Necchi, Synthesis, characterization and antibacterial activity against Gram positive and Gram negative bacteria of biomimetically coated silver nanoparticles, *Langmuir*, 2011, 27 (15), 9165

35 M.-J. Bañuls, R. Puchades, and Á. Maquieira, Chemical surface modifications for the development of silicon-based label-free integrated optical (IO) biosensors: A review, *Analytica Chimica Acta*, 2013, 777, 1

36 F. Wu, and Cees Dekker, Nanofabricated structures and microfluidic devices for bacteria: from techniques to biology, *Chem. Soc. Rev*., 2016, 45,268

37 T. A. Cameron, J. R. Zupan, and P. C. Zambryski, The essential features and modes of bacteria polar growth, *Trends in Microbiology*, 2015, 23(6), 347

38 P. J. B. Brown, D. T. Kysela, and Y. V. Brun, Polarity and the diversity of growth mechanisms in bacteria, *Semin. Cell. Dev. Biol.*, 2011, 22(8), 790

39 T. J. Silhavy, D. Kahne, and S. Walker, The Bacterial Cell Envelope, *Cold. Spring. Harb. Perspect. Biol.*, 2010, 2(5), a000414

40 K. J. Anusavice, N.-Z. Zhang, and C. Shen, Controlled release of chlorhexidine from UDMA-TEGMA resin, *J. Dent. Res.*, 2006, 85(10), 950

41 H.-Y. Cheung, M. M.-K. Wong, S.-H. Cheung, L. Y. Liang, Y.-W. Lam, S.-K. Chiu, Differential actions of chlorhexidine on the cell wall of *Bascillus subtillis* and *Escherichia coli*, 2012, 7(5), e36659